THE JOURNAL OF PHYSICAL CHEMISTRY C
A JOURNAL OF THE AMERICAN CHEMICAL SOCIETY

pubs.acs.org/JPCC
Article

Potential-Dependent and Face Orientation-Dependent Electrochemical Oxidative Desorption Behavior of Sulfur Species Adsorbed on Platinum Single-Crystal Surfaces

Tetsuro Morooka, Tamao Shishido, Ruttala Devivaraprasad, Ganesan Elumalai, Makoto Aoki, Tetsuroh Shirasawa, Takuya Nakanishi, Atsushi Ishikawa, Toshihiro Kondo, and Takuya Masuda*

Cite This: J. Phys. Chem. C 2024, 128, 16426−16436

ABSTRACT: We investigated the effect of surface atomic arrangements of electrodes on electrochemical oxidative desorption behavior of sulfur species at Pt single-crystal electrodes with face orientations of (111), (110), and (100) by electrochemical measurements, X-ray photoelectron spectroscopy (XPS), and density functional theory (DFT) calculations. Upon the adsorption of elemental sulfur, electrochemical responses characteristic to Pt(111), Pt(110), and Pt(100) electrodes in aqueous electrolytes such as adsorption/desorption of hydrogen and hydroxyl species completely disappeared, and S 2p peaks attributed to the adsorbed sulfur appeared in XPS at each electrode. Those surface-structure-dependent electrochemical responses gradually recovered, simultaneously with the decrease of S 2p peaks, by cycling to or holding at positive potentials due to the oxidative desorption of adsorbed sulfur. The recovery of the electrochemically active surface area (ECSA) was promoted by keeping the potential more positive for a longer period. Among the three different face orientations, the oxidative desorption of sulfur started from the least positive potential at the Pt(111) electrode in both experiments, showing that the atomic arrangement of the Pt(111) electrode is most advantageous for the recovery of ECSA from sulfur poisoning. In the potential holding experiment, the oxidative desorption of sulfur occurred at less positive potential at the Pt(111), Pt(100), and Pt(110) electrodes in that order. One of the mechanistic reasons is explained with the DFT calculations, which evidenced that the adsorption energies of SO_2 at the Pt(111), Pt(100), and Pt(110) electrodes are in the same order. This correlation suggests that the desorption of SO_2 formed by the oxidation of the adsorbed sulfur is an important step. In the potential cycling experiment, however, the oxidative desorption of sulfur more easily occurred at the Pt(111), Pt(110), and Pt(100) electrodes in that order. Once the adsorbed sulfur is oxidized to SO_2, SO_2 desorbs from the surface or remains at the surface to be subsequently reduced to elemental sulfur in the negative potential scan. Since the reduction of SO_2 to elemental sulfur more easily occurs at Pt(100) than at the other two electrodes, the recovery of ECSA at the Pt(100) electrode became slower in the potential cycling experiment. Thus, the fate of SO_2 formed by the oxidation of sulfur is one of the important factors affecting the recovery rate of ECSA from sulfur poisoning.

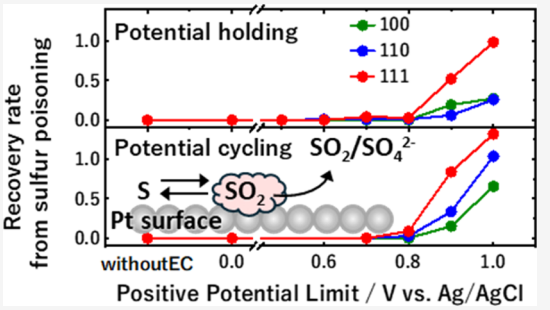

1. INTRODUCTION

Polymer electrolyte membrane fuel cells (PEMFCs) are a promising technology to convert chemical energy to electrical energy with very high theoretical efficiency.[1] In PEMFCs, supplied hydrogen is oxidized in the anode, while oxygen from the air is reduced in the cathode, and these multielectron transfer reactions occur at the surface of the platinum (Pt) electrocatalyst.[2,3] However, the cell performance of PEMFCs is severely degraded by the adsorption of pollutants and impurities present in air and hydrogen fuel gas.[4] Because sulfur species such as elemental S, H_2S, C_2S, COS, and SO_2 strongly adsorb on the surface of Pt electrocatalysts to suppress or rather enhance the electrochemical processes,[1,5−12] understanding and control of adsorption/desorption behavior of sulfur species at Pt surfaces are especially important to sustain the inherent cell performance of PEMFCs.

In the 1980s and 1990s, the structures of sulfur adlayer with less than a monolayer (ML) coverage at Pt single-crystal surfaces have been studied on an atomic scale from the fundamental point of view.[13−17] These studies determined well-ordered atomic arrangements of adsorbed sulfur, such as $(\sqrt{3} \times \sqrt{3})$-R30° (0.3 ML) at the Pt(111),[13,16,17] $p(4 \times 4)$ (0.8 ML) at the Pt(110),[14] and $(\sqrt{2} \times \sqrt{2})$-R45° (0.5 ML) at the Pt(100) surfaces,[13,15] by various surface characterization techniques

Received: May 15, 2024
Revised: August 9, 2024
Accepted: September 5, 2024
Published: September 19, 2024

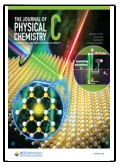

https://doi.org/10.1021/acs.jpcc.4c03227
J. Phys. Chem. C 2024, 128, 16426−16436

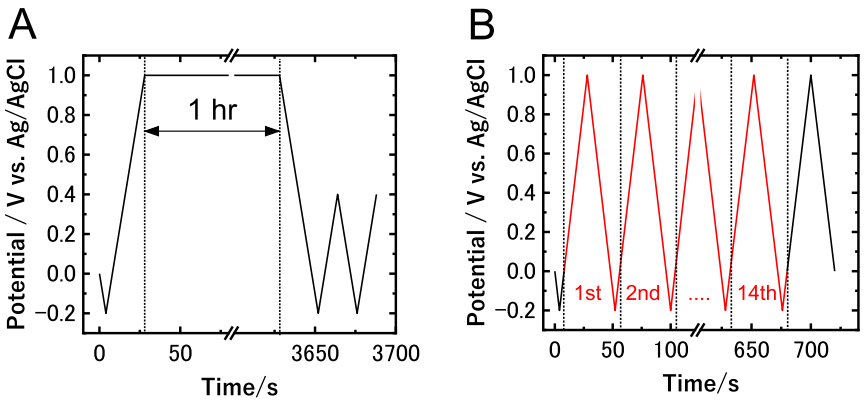

Figure 1. Potential regulation for (A) potential holding and (B) potential cycling experiments (corresponding to the case where the positive potential limit is set to 1.0 V).

including low-energy electron diffraction[13,14] and scanning tunneling microscopy.[15−17]

Afterward, the electro-oxidation behavior of sulfur at Pt surfaces has been extensively studied by using Pt nanoparticles supported on carbon electrodes, from a perspective of mitigation of sulfur poisoning in PEMFCs.[8,9,18−23] However, the surfaces of Pt nanoparticles are mostly composed of (111) and (100) facets together with their steps/kinks/ledges under thermodynamic equilibria, and thus, averaged information for a variety of reaction active sites can be obtained from electrochemical and spectroscopic analyses using Pt nanoparticles.

Recently, to understand the site-dependent electro-oxidation mechanism of sulfur, a few groups have revisited the fundamental electrochemical properties of Pt single-crystal electrodes with different face orientations in the presence of sulfur species.[13,24−27] The adsorption of sulfur on the Pt(111) surface caused the almost complete disappearance of characteristic current responses in sulfuric acid corresponding to the adsorption/desorption of hydrogen and hydroxyl species, while the oxidative desorption of sulfur by the electrochemical potential cycling in the range of −0.28 to +0.82 V vs Ag/AgCl led to the recovery of those current responses.[24,25] It should be noted that although the adsorbed structures of sulfur on each of the Pt(111), Pt(110), and Pt(100) single-crystal surfaces were fully determined on an atomic scale,[13−17,24,25] their effects on the oxidative desorption behavior are not fully understood.

In the present work, we further systematically studied the potential-dependent and face orientation-dependent adsorption/desorption behavior of sulfur at the Pt(111), Pt(110), and Pt(100) single-crystal electrodes by electrochemical measurements in perchloric acid, X-ray photoelectron spectroscopy (XPS), surface X-ray diffraction (SXRD), and density functional theory (DFT) calculations to explicitly clarify the oxidative desorption mechanism about PEMFCs.

2. METHODS

2.1. Materials. The Pt(111), Pt(110), and Pt(100) single-crystal disks (99.99%, diameter:10 mm, thickness: 5 mm) were purchased from the Surface Preparation Laboratory. Ultrapure reagent-grade $HClO_4$ (60%) and reagent-grade Na_2S (98.0%) were purchased from Wako Pure Chemicals, and first-grade 5% SO_2 aqueous solution purchased from Sigma-Aldrich was used without further purification. Water was purified using a Milli-Q system (ELGA LabWater). Ultrapure Ar (99.999%)/H_2 (99.999%) mixed gases (95:5) were purchased from Suzuki Shokan.

2.2. Sample Preparation. Prior to each measurement, the Pt single-crystal electrodes were annealed using an induction heater at 1600 °C for more than 1 h under the flowing Ar/H_2 mixed gas.[28−31] After cooling under the flowing Ar/H_2 mixed gas for 7 min, the clean Pt single-crystal electrodes were immersed in a 1 mM Na_2S aqueous solution under the flowing Ar/H_2 mixed gas for 1 h to form S-adsorbed Pt single-crystal electrodes. After being rinsed with water, those S-adsorbed Pt single-crystal electrodes were transferred to the electrochemical cell filled with an S-free 0.1 M $HClO_4$ aqueous electrolyte solution, with a droplet of water kept on the surface to avoid any surface contamination.

2.3. Electrochemical Measurements. Electrochemical measurements were performed at room temperature by using a three-electrode electrochemical cell in the hanging-meniscus configuration. An Ag/AgCl electrode (saturated NaCl, +0.200 V vs RHE),[32,33] Pt wire, and the Pt single-crystal electrodes were used as a reference, counter, and working electrode, respectively. The potential of the working electrode was controlled by a potentiostat (Hokuto Denko, HAB-151A). Potential-dependent current responses were recorded by using a data logger (Graphtec, GL900). Cyclic voltammetry (CV) measurements of the Pt single-crystal electrodes were carried out in an S-free 0.1 M $HClO_4$ aqueous electrolyte solution deaerated by ultrapure Ar gas, unless otherwise specified. To clarify the mechanism of oxidative desorption, the electrode potential was regulated in two ways: (1) potential holding at "positive potential limit" for 1 h followed by cycling to the less positive potential and (2) potential cycling to the positive potential limit, for both of which the negative potential limit was set to −0.2 V (Figure 1).

2.4. XPS Measurements. XPS measurements were performed using AXIS-NOVA (Shimadzu Kratos) equipped with a monochromatic Al Kα source at an operating X-ray power of 300 W without charge neutralization. The photoelectron takeoff angle was fixed at 90°. The analysis area was a spot with a diameter of 110 μm, and the energy of the photoelectrons passing through the analyzer (pass energy) was 80 eV. The vacuum pressure in the analysis chamber was $\sim 1.5 \times 10^{-8}$ Torr. The position of the Pt $4f_{7/2}$ peak was calibrated to 71.2 eV, and the intensity of the S 2p peak was normalized by dividing by that of the Pt 4f peak of the same sample.

2.5. SXRD Measurements. The SXRD measurements were carried out using a spectroelectrochemical cell as previously reported.[31,34] The electrode potential was controlled with a potentiostat/galvanostat (Hokuto Denko, HA-151), and an

https://doi.org/10.1021/acs.jpcc.4c03227
J. Phys. Chem. C 2024, 128, 16426−16436

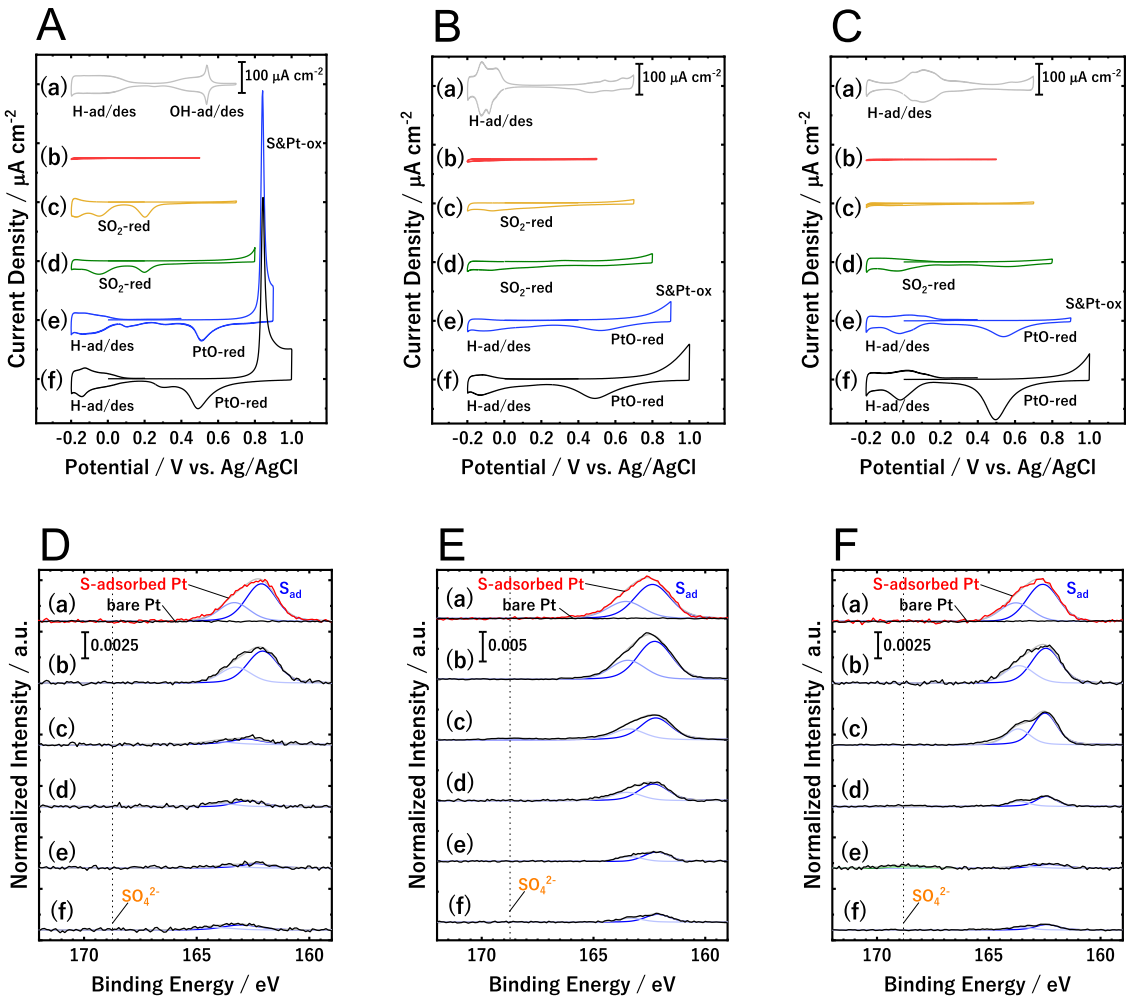

Figure 2. Cyclic voltammograms of (a) bare and S-adsorbed (A) Pt(111), (B) Pt(110), and (C) Pt(100) electrodes measured in a 0.1 M $HClO_4$ aqueous solution with a scan rate of 50 mV s^{-1} accompanied by preceding potential holding at (b) 0.5, (c) 0.7, (d) 0.8, (e) 0.9, and (f) 1.0 V for 1 h. Photoelectron spectra in the S 2p region of (a) bare and S-adsorbed (D) Pt(111), (E) Pt(110), and (F) Pt(100) electrodes obtained (a) before and after the CV measurements accompanied by preceding potential holding at (b) 0.5, (c) 0.7, (d) 0.8, (e) 0.9, and (f) 1.0 V.

external potential was provided by a function generator (Hokuto Denko, HB-111). A Pt wire and Ag/AgCl (saturated NaCl, +0.200 V vs RHE)[32,33] electrode were used as a counter and reference electrode, respectively. The spectroelectrochemical cell was set on a four-circle diffractometer (HUBER, type 5020) installed in an undulator beamline BL3A at the Photon Factory. The intensity of the incident X-rays was measured by an ion chamber, which was placed in front of the sample, to normalize the intensity of diffracted X-rays. The incident X-ray energy of 11.27 keV (wavelength: 1.10 Å) was selected to avoid any fluorescence background from the Pt electrode. An energy-sensitive silicon drift detector was used to detect diffracted X-rays. For the SXRD measurements, hexagonal, square, and rectangular coordinate systems in which H and K are parallel to the surface and L is normal to the surface were used at (111), (100), and (110) surfaces. The SXRD profiles were measured at L = 0.2 (incident angle: ca. 0.3−0.6°).

2.6. Computational Details. The Pt(111), Pt(110), and Pt(100) surfaces were constructed from the bulk Pt. The lattice constants of the Pt bulk were optimized with the DFT. This procedure gives the lattice constant of 3.92 Å, which is in good agreement with the experimental value (3.91 A).[35] For the lateral directions, a 3 × 3 supercell was taken for Pt(111), while a 2 × 2 supercell was taken for Pt(110) and Pt(100). Eight atomic layers were taken for all surfaces. The number of Pt atoms was 72, 32, and 32 for Pt(111), Pt(110), and Pt(100). For these surface models, the lower two atomic layers were fixed during the geometry optimization, and other layers were fixed to mimic the bulk behavior. The adsorption site of SO_2 is determined according to the previous theoretical study.[36]

In the DFT calculations, the core electrons were represented by the projector augmented-wave method,[37] and the valence electrons were expanded by the plane wave basis set up to a cutoff energy of 500 eV. Several exchange−correlation functions were examined in this work: PBE,[38] PBE-D3 with Becke−Johnson damping,[38,39] vdw-DFT,[40] BEEF-vdw,[41] and opt-PBE functionals,[42] as these functionals are relatively more accurate than the standard generalized gradient approximation functionals. The optimization of bulk Pt was done with the PBEsol functional.[43] The first-order Methfessel−Paxton scheme with σ = 0.01 was used for smearing the electron occupation near the Fermi level. The convergence thresholds for the electronic state calculation and geometry optimization were set to 1.0×10^{-5} eV and 0.03 eV/Å in energy and force, respectively (in the bulk Pt optimization, the convergence threshold of ion relaxation was set to 1.0×10^{-6} eV in energy). Integration in the reciprocal lattice space was performed by numerical integration using k-points, which were placed such that the spacing between them

https://doi.org/10.1021/acs.jpcc.4c03227
J. Phys. Chem. C 2024, 128, 16426−16436

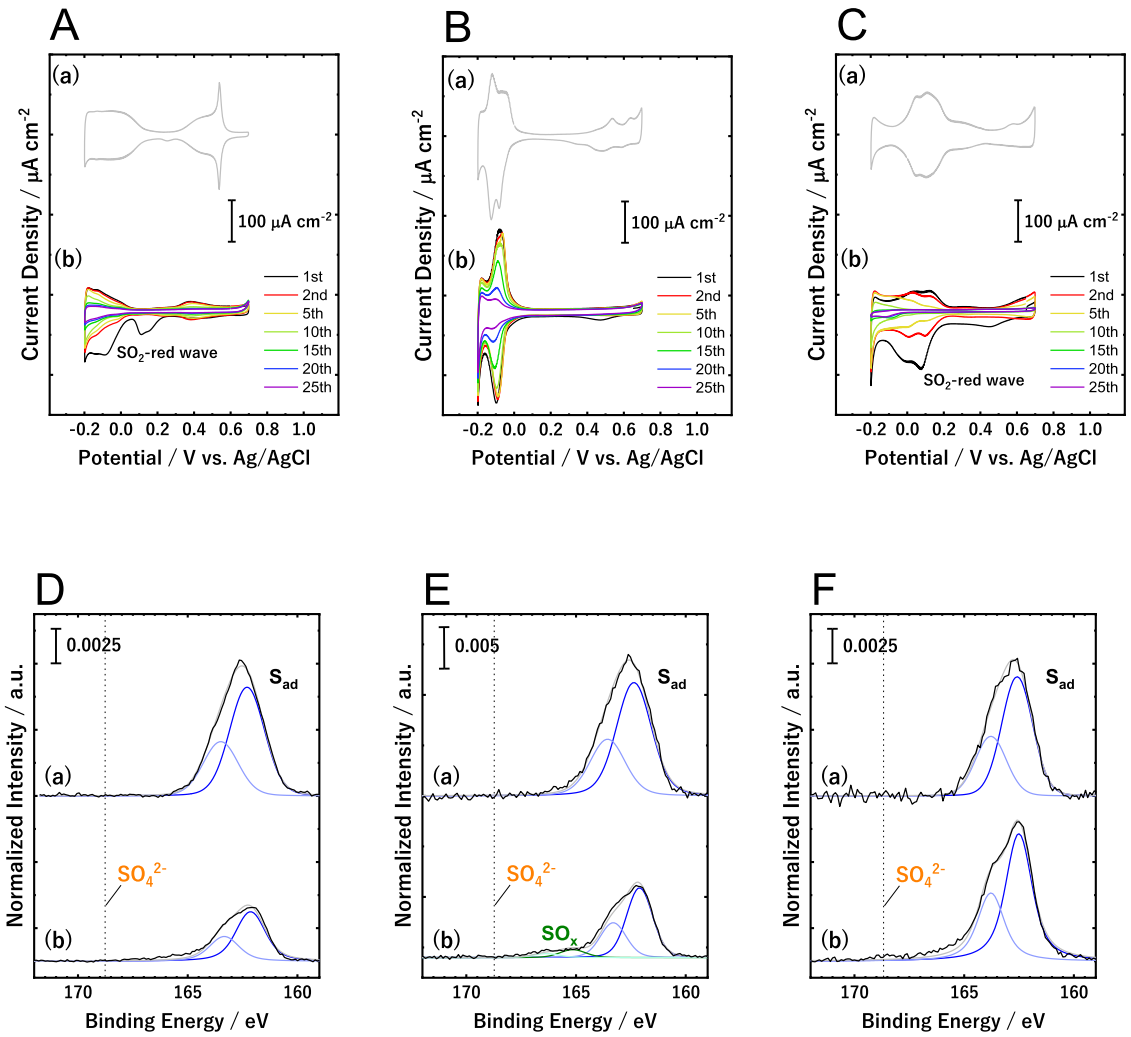

Figure 3. Cyclic voltammograms of S-free bare (A) Pt(111), (B) Pt(110), and (C) Pt(100) electrodes measured in a 0.1 M $HClO_4$ aqueous solution (a) without and (b) with 1 mM SO_2 with a scan rate of 50 mV s^{-1}. For the cyclic voltammograms measured in a 1 mM SO_2-containing solution, 1st (black), 2nd (red), 5th (yellow), 10th (light green), 15th (green), 20th (blue), and 25th cycles (purple) were shown. Photoelectron spectra in the S 2p region of (D) Pt(111), (E) Pt(110), and (F) Pt(100) electrodes obtained after (a) immersing in a 1 mM Na_2S aqueous solution under the flowing Ar/H_2 mixed gas for 1 h and (b) potential cycling in a 0.1 M $HClO_4$ aqueous solution containing 1 mM SO_2 with the positive potential limit of 0.7 V for 25 times.

was 0.3 $Å^{-1}$, while in the bulk Pt optimization, the spacing was set to 0.1 $Å^{-1}$. The gamma point was always included. For an isolated molecule, i.e., SO_2 calculation, a single *k*-point was placed on the gamma point. A vacuum layer with a thickness of 12 Å was placed between the slabs, and a dipole correction in the *z*-direction was introduced to remove the artificial interaction between the slabs. All the calculations were performed with the Vienna ab initio simulation package (VASP) version 5.4.[44,45] The visualization of the molecular or surface structures was made with VESTA software.[46]

3. RESULTS AND DISCUSSION

3.1. Electrochemical Properties of Bare and S-Adsorbed Pt Surfaces and Potential Holding Experiment. Figure 2A–C shows cyclic voltammograms of bare and S-adsorbed Pt(111), Pt(110), and Pt(100) electrodes in a 0.1 M $HClO_4$ aqueous solution obtained after keeping the potential at the various positive potential limits for 1 h. The cyclic voltammogram of the bare Pt(111) electrode (Figure 2A(a), gray) showed characteristic current responses attributed to adsorption/desorption of hydrogen (−0.20 to +0.15 V, reaction 1) and hydroxyl species (+0.30 to +0.60 V, reaction 2).[29,47] The cyclic voltammograms of bare Pt(110) (Figure 2B(a), gray) and Pt(100) electrodes (Figure 2C(a), gray) were also identical to those of the literature.[29,47]

$$Pt + H^+ + e^- \rightarrow Pt - H \quad (1)$$

$$Pt + H_2O \rightarrow Pt - OH + H^+ + e^- \quad (2)$$

After the treatment with Na_2S solution, those characteristic current responses in cyclic voltammograms completely disappeared at each electrode (Figure 2A–C(b), red), indicating the blocking of adsorption/desorption of hydrogen and hydroxyl species due to the presence of adsorbed sulfur. Corresponding to these changes in cyclic voltammograms, a doublet peak assignable to the elemental sulfur adsorbed on Pt appeared at 162.4 and 163.6 eV in the S 2p region of photoelectron spectra for all of Pt(111), Pt(100), and Pt(110) electrodes (Figure 2D–F(a), red).[48−50] The normalized peak intensity of adsorbed sulfur at the Pt(110) electrode (Figure 2E(a), red) was somewhat larger than those at (nearly twice

https://doi.org/10.1021/acs.jpcc.4c03227
J. Phys. Chem. C 2024, 128, 16426−16436

those of) the Pt(111) (Figure 2D(a), red) and Pt(100) electrodes (Figure 2F(a), red). This is in reasonable agreement with the coverages of sulfur, i.e., the ratios of the number of surface S and Pt atoms, 0.3 ML at the Pt(111) electrode with the $(\sqrt{3} \times \sqrt{3})$-R30° structure,[13,16,17] 0.8 ML at the Pt(110) electrode with the $p(4 \times 4)$ structure,[14] and 0.5 ML at the Pt(100) electrode with the $(\sqrt{2} \times \sqrt{2})$-R45° structure,[13,15] as summarized in Table S1 in the Supporting Information. It is noted that the intensities and positions of S 2p peaks shown in Figure 2D−F were calibrated by those of Pt 4f peaks of the same samples. In addition, the adsorbed structures of sulfur, $(\sqrt{3} \times \sqrt{3})$-R30° at the Pt(111) and $(\sqrt{2} \times \sqrt{2})$-R45° at the Pt(100) electrodes, were evident by the SXRD peaks at $(0\ 2/\sqrt{3}\ 0.2)$ and $(0\ 1/\sqrt{2}\ 0.2)$ reciprocal lattice points, respectively, as shown in Figure S1 in the Supporting Information.

$$S + xH_2O \rightarrow SO_x + 2xH^+ + ye^- \quad (3)$$

$$S + 2H_2O \rightarrow SO_2 + 4H^+ + 4e^- \quad (4)$$

$$S + 4H_2O \rightarrow SO_4^{2-} + 8H^+ + 6e^- \quad (5)$$

The potential holding at 0.5 V did not cause much change in the cyclic voltammograms (Figure 2A−C(b), red) and photoelectron spectra of the S 2p region (Figure 2D−F(b)). When the holding potential became more positive, however, the oxidation current started to flow at around 0.6 V at the Pt(111), Pt(110), and Pt(100) electrodes (the cyclic voltammograms shown in Figure 2A−C(d−f) are magnified in Figure S2A−C in the Supporting Information). These oxidation currents should be due to the electrochemical oxidative desorption of adsorbed sulfur (reactions 3−5)[23] because the intensities of S 2p peaks substantially decreased after the potential holding at 0.7 V or more positive (Figure 2D−F(c−f), yellow to black).

The oxygen source for the oxidation of elemental sulfur is considered to be oxygen species adsorbed on the Pt surfaces, such as hydroxyl species and water molecules. The adsorbed amounts of oxygen species at "bare" Pt(111), Pt(110), and Pt(100) single-crystal electrodes after electrochemical treatments at various electrode potentials were systematically studied by electrochemical-XPS.[51] The electrochemical-XPS showed that, at all the face orientations, adsorbed OH and/or H_2O was detected after the electrochemical treatment at 0.5 V vs RHE (~0.3 V vs Ag/AgCl) or more positive. In the present study, the Pt(111), Pt(110), and Pt(100) surfaces were covered by the adsorbed sulfur before the electrochemical measurements in $(\sqrt{3} \times \sqrt{3})$-R30° with a coverage of 0.3 ML,[13,16,17] $p(4 \times 4)$ with a coverage of 0.8 ML,[14] and $(\sqrt{2} \times \sqrt{2})$-R45° with a coverage of 0.5 ML,[13,15] respectively. According to the adsorbed structure of sulfur at each surface (Figure S1), however, there are still sufficient vacant adsorption sites for oxygen species.

Moreover, current waves (−0.1 to +0.3 V) attributable to the reduction of SO_2 to elemental sulfur or sulfur interacting with Pt (see below in Figure 3, reaction 6)[52] were clearly observed in the negative going scan after the potential holding at 0.7 V (Figure 2A−C(c), yellow), especially at the Pt(111) electrode (Figure 2A(c), yellow).

$$SO_2 + 4H^+ + 4e^- \rightarrow S + 2H_2O \quad (6)$$

These results show that the adsorbed sulfur is oxidized to SO_2 and/or SO_4^{2-} at 0.7 V or more positive, and then some of those oxidized sulfur species desorb from the Pt surface and diffuse into the bulk solution, while the remaining SO_2 at the Pt surface is reduced to the adsorbed sulfur.

After holding the potential at 0.7 V for 1 h, where the oxidation currents were barely observed at the S-adsorbed Pt(111) electrode (Figure 2A(c), yellow and magnified in Figure S2A), the S 2p peaks almost disappeared at the Pt(111) electrode (Figure 2D(c)). When the positive potential limit, i.e., holding potential, was extended to 0.9 V or more positive at the Pt(111) electrode (Figure 2A(e,f), blue and black), a sharp oxidation peak was observed at around 0.84 V in the positive going scan, and a broad reduction peak of Pt oxide was observed at around 0.5 V in the negative going scan, as well as the recovered current waves due to the adsorption/desorption of hydrogen and hydroxyl species. This confirms that the above-mentioned sharp peak is due to the oxidation of sulfur and the Pt electrode, which brings about the recovery of the electrochemically active surface area (ECSA). The difference between the charge integration of the sharp sulfur oxidation peak at 0.84 V, 423 μC cm^{-2}, and that of the broad Pt oxide reduction peak at 0.5 V, 58 μC cm^{-2}, was in reasonable agreement with the theoretical charge density of four-electron oxidation of sulfur adsorbed on the Pt(111) surface in the $(\sqrt{3} \times \sqrt{3})$-R30° structure, 322 μC cm^{-2}, implying that the major oxidation product is SO_2 (reaction 4).

The oxidative desorption of sulfur at the Pt(110) and Pt(100) electrodes occurred at a more positive potential than at the Pt(111) electrode. After holding the potential of the S-adsorbed Pt(110) electrode at 0.7 V, current wave due to the SO_2 reduction appeared in the CV (Figure 2B(c), yellow) and S 2p peaks substantially decreased (Figure 2E(c)). In the case of the S-adsorbed Pt(100) electrode, the SO_2 reduction current and the decrease of S 2p peaks were barely observed after holding the potential at 0.7 V [Figure 2C(c), yellow and Figure 2F(c)] but more pronounced at 0.8 V [Figure 2C(d), green and Figure 2F(d)]. The oxidative desorption of sulfur at the Pt(110) and Pt(100) electrodes was almost completed by holding the potential at 1.0 V [Figure 2E(f)] and 0.9 V [Figure 2F(e)] for 1 h, respectively.

It is noted that, after the potential holding at 0.9 V or more positive [Figure 2A−C(e,f), blue and black], the shape of current waves due to the adsorption/desorption of hydrogen and hydroxyl species were substantially different from those of original bare electrodes because the original surface atomic arrangements of the Pt(111), Pt(110), and Pt(100) electrodes were severely compromised due to the oxidation and successive reduction.[51,53−56]

3.2. Electrochemical Reduction of SO_2 to Elemental Sulfur at Bare Pt Surfaces. Figure 3A−C shows cyclic voltammograms of S-free bare Pt(111), Pt(110), and Pt(100) electrodes in a 0.1 M $HClO_4$ aqueous solution containing 1 mM SO_2, together with those without 1 mM SO_2 for comparison. At the Pt(111) electrode, current waves attributed to the reduction of SO_2 were certainly observed in the potential range of −0.1 to +0.3 V in the negative going scan of the first cycle (Figure 3A(b), black),[52] together with hydrogen adsorption/desorption waves (−0.2 to +0.15 V). In the second cycle (Figure 3A(b), red), the SO_2 reduction waves significantly decreased, while the hydrogen adsorption/desorption waves remained. Increasing the number of potential cycling between −0.2 and +0.7 V (Figure 3A(b), yellow to purple), however, the hydrogen adsorption−desorption waves gradually decreased. Figure 3D−F shows the XPS results of the relevant specimens. After the potential cycling for 25 times, a doublet peak due to the adsorbed elemental sulfur, not oxidized sulfur species such as SO_2, SO_3, and SO_4^{2-}, was observed in the S 2p region of the photoelectron spectrum

https://doi.org/10.1021/acs.jpcc.4c03227
J. Phys. Chem. C 2024, 128, 16426−16436

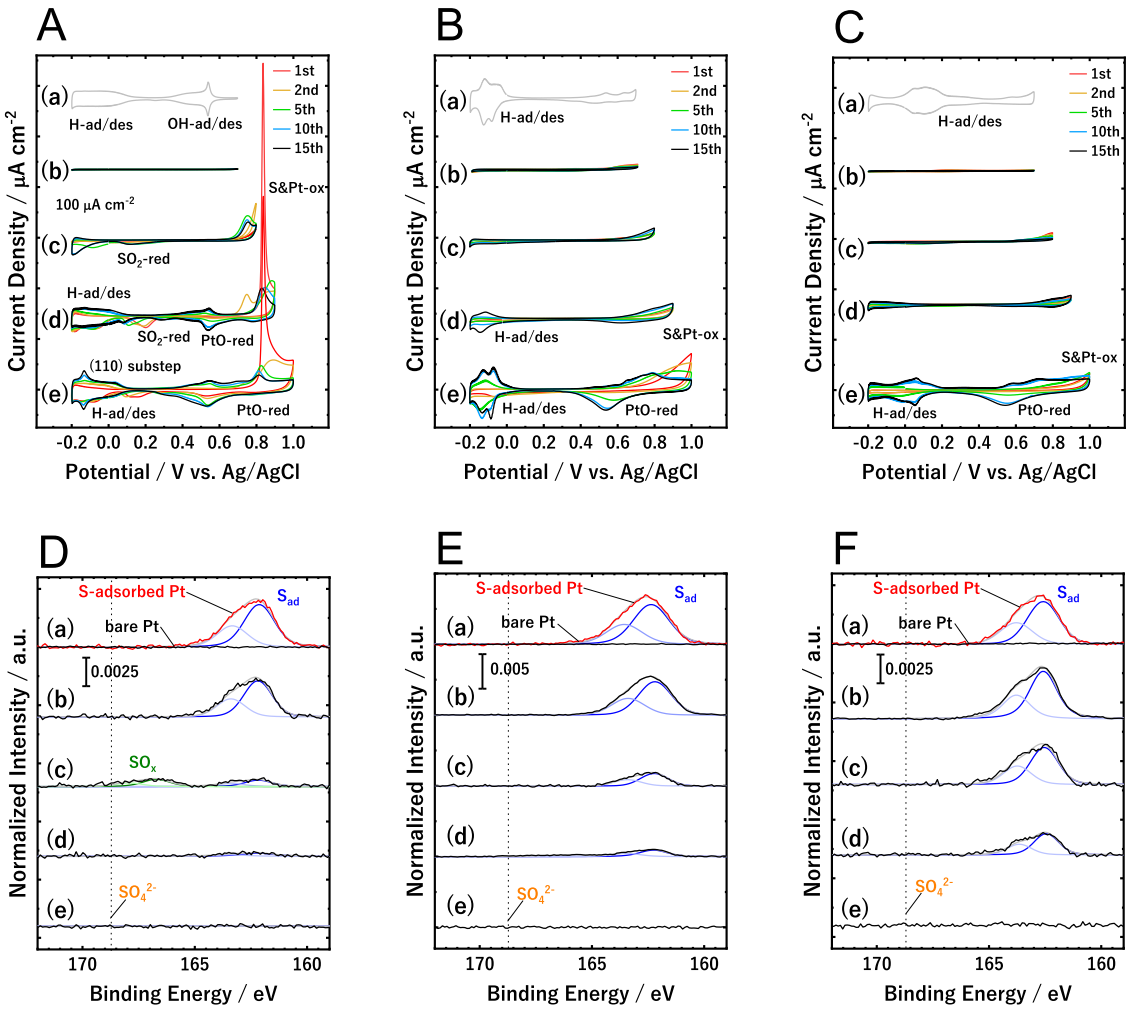

Figure 4. Cyclic voltammograms of (a) bare and S-adsorbed (A) Pt(111), (B) Pt(110), and (C) Pt(100) electrodes measured in a 0.1 M $HClO_4$ aqueous solution with a scan rate of 50 mV s^{-1}, with the positive potential limits of (b) 0.7, (c) 0.8, (d) 0.9, and (e) 1.0 V. For the cyclic voltammograms of S-adsorbed Pt electrodes, 1st (red), 2nd (yellow), 5th (green), 10th (blue), and 15th cycles (black) were shown. Photoelectron spectra in the S 2p region of (a) bare and S-adsorbed (D) Pt(111), (E) Pt(110), and (F) Pt(100) electrodes obtained (a) before and after the potential cycling with the positive potential limit of (b) 0.7, (c) 0.8, (d) 0.9, and (e) 1.0 V for 14 times.

[Figure 3D(b)]. Although the SO_2 reduction waves in cyclic voltammograms at the Pt(110) [Figure 3B(b), black] and Pt(100) electrodes [Figure 3C(b), black] were not as clear as that at the Pt(111) electrode [Figure 3A(b), black], S 2p peaks originating from the adsorbed elemental sulfur were observed in the photoelectron spectra of the Pt(110) [Figure 3E(b)] and Pt(100) electrodes [Figure 3F(b)] after the potential cycling for 25 times. These results confirm that some of the oxidatively formed SO_2 can be reduced to adsorbed sulfur in the negative going scan.

At the Pt(111) [Figure 3D(b)] and Pt(110) electrodes [Figure 3E(b)], the intensities of S 2p peaks, i.e., the adsorbed amount of sulfur after the potential cycling in the SO_2-containing solution, were somewhat smaller than those at the Pt(111) [Figure 3D(a)] and Pt(110) electrodes [Figure 3E(a)] immersed in a 1 mM Na_2S aqueous solution, respectively. In contrast, the intensities of S 2p peaks at the Pt(100) electrodes after immersion in a 1 mM Na_2S aqueous solution [Figure 3F(a)] and the potential cycling in the SO_2-containing solution [Figure 3F(b)] were almost the same as each other. These results suggest that the SO_2 reduction and resulting readsorption of sulfur are more likely to occur at the Pt(100) electrode than at the Pt(111) and Pt(110) electrodes.

3.3. Electrochemical Properties of Bare and S-Adsorbed Pt Surfaces and Potential Cycling Experiment.

Figure 4 shows cyclic voltammograms of bare and S-adsorbed Pt(111), Pt(110), and Pt(100) electrodes in a 0.1 M $HClO_4$ aqueous solution in the various potential ranges (A–C) with the related XPS results (D–F). As is the case of the potential holding experiment (Figure 2), current responses characteristic to the bare Pt(111), Pt(110), and Pt(100) electrodes [Figure 4A–C(a), gray] completely disappeared after the adsorption of sulfur [Figure 4A–C(b), black], and a doublet peak corresponding to the adsorbed sulfur appeared in the S 2p region of photoelectron spectra [Figure 4D–F(a)]. The potential cycling for 15 times with a positive potential limit of 0.7 V did not change the cyclic voltammograms [Figure 4A–C(b), red to black] and photoelectron spectra of the S 2p region [Figure 4D–F(b)], confirming the blocking of adsorption/desorption of hydrogen and hydroxyl species by the adsorbed sulfur. It is noted that, in the potential cycling experiment (Figure 4A–C), the oxidative desorption of sulfur and recovery of electrochemical current responses occurred with more positive potential limits than in

https://doi.org/10.1021/acs.jpcc.4c03227
J. Phys. Chem. C 2024, 128, 16426–16436

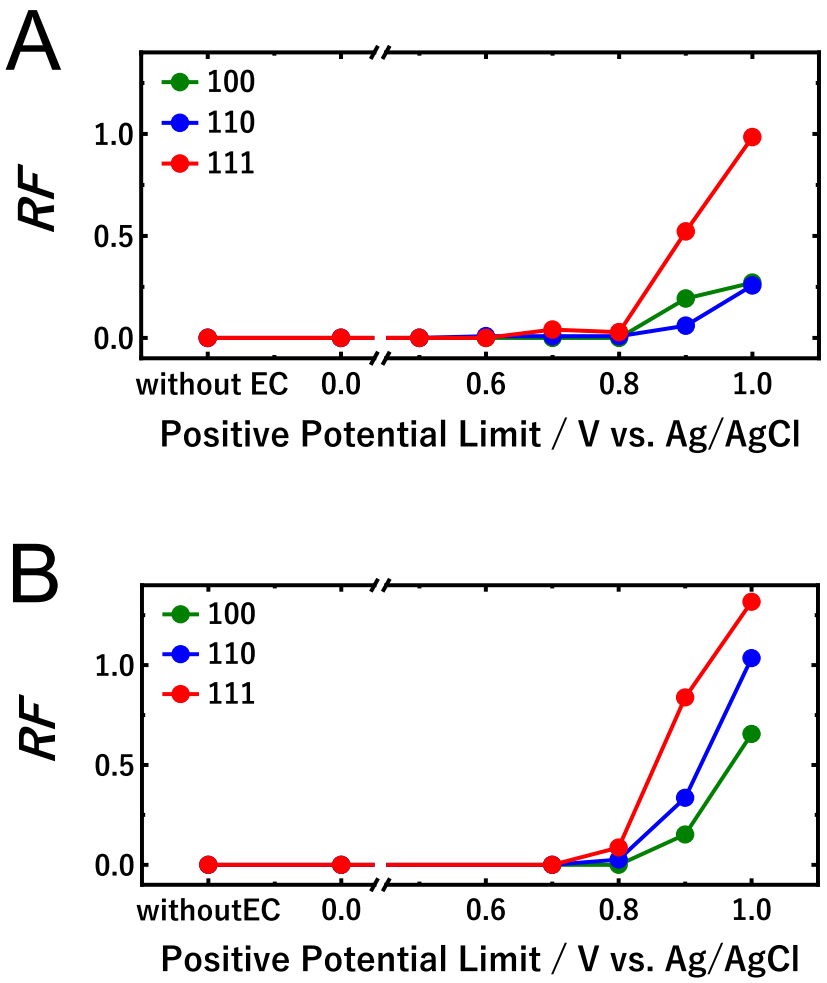

Figure 5. Recovery factor, RF, for (A) potential holding and (B) potential cycling experiments of the S-adsorbed Pt(111), Pt(110), and Pt(100) electrodes with respect to the positive potential limit.

the potential holding experiment (Figure 2A–C) because the potential holding experiment kept the potential at the positive limit for a longer period than the potential cycling experiment, as shown in Figure 1.

After the potential cycling with the positive limit of 0.8 V for 15 times [Figure 4A–C(c), red to black], the S 2p peaks decreased significantly at the Pt(111) [Figure 4D(c)] and Pt(110) electrodes [Figure 4E(c)] and slightly at the Pt(100) electrode [Figure 4F(c)]. Only at the Pt(111) electrode after the potential cycling up to 0.8 V for 15 times, a new S 2p peak appeared at 166.7 eV [Figure 4D(c)], assignable to the oxidatively formed sulfur oxides such as SO_2 and SO_3, which can specifically adsorb on the Pt surfaces.[57] As the positive potential limit became 0.9 V or more positive, the current responses due to the adsorption/desorption of hydrogen and hydroxyl species gradually recovered with the number of cycles [Figure 4A–C(d,e), red to black]. Thus, the increase of the current responses, i.e., recovery of ECSA, and decrease of the S 2p peak intensity, i.e., desorption of sulfur, became more pronounced as the number of cycles increased and/or the positive potential limit became more positive. After the potential cycling up to 1.0 V for 15 times [Figure 4A–C(e), red to black], the increase of ECSA and changes in cyclic voltammograms from those of original bare Pt(111), Pt(110), and Pt(100) electrodes due to the change in their atomic arrangement were more significant than those of the potential holding experiment [Figure 2A–C(f), black]. Especially, a new reversible peak appeared at around −0.15 V at the Pt(111) electrode [Figure 4A(e), black] due to the formation of the (110) substep.[58−60] These results show that the roughening of Pt surfaces was accelerated by repeating place-exchange of oxygen and Pt accompanying oxidation/reduction cycles when the potential was swept up to the potential range where Pt oxide was formed.[61]

One may be concerned that the surface roughening affects the oxidative desorption of sulfur at the Pt surfaces because the created defect sites can alter the adsorption behavior of sulfur and oxygen species. This effect can be discussed by using the cyclic voltammograms of the Pt(111) electrode with the positive potential limit of 1.0 V [Figure 4A(e)] as an example. The current peak due to the reduction of Pt oxide at 0.5 V was very small in the first potential cycling up to 1.0 V [Figure 4A(e), red], showing that the Pt oxide formation was rather suppressed by the adsorbed sulfur. In addition, the hydrogen adsorption/desorption current recovered up to ∼60% in the second potential cycling [Figure 4A(e), yellow] while maintaining the characteristic shape of hydrogen adsorption/desorption waves at the Pt(111) electrode. Thus, the oxidative desorption of sulfur occurs prior to the surface roughening caused by repeating the Pt oxide formation and reduction. Furthermore, it was reported that S species rather preferentially adsorb on the flat terrace.[62]

https://doi.org/10.1021/acs.jpcc.4c03227
J. Phys. Chem. C 2024, 128, 16426−16436

Accordingly, the effect of surface roughening is considered to be not significant.

3.4. Recovery from the Sulfur Poisoning and Their Face Orientation Dependence at Pt Surfaces. Due to the significant importance of the oxidative desorption of sulfur from Pt(111), Pt(110), and Pt(100), which can be varied with different electrochemical treatments (i.e., potential holding or cycling, positive potential limit), for the use of Pt electrodes in the fuel cells, the recovery factor (RF) is defined as follows (equation 7) based on the electrochemical charge integrations of hydrogen desorption at the Pt electrodes (Figure S3 in the Supporting Information).

$$\mathrm{RF} = \frac{C_{\mathrm{S-adsorbed},X}}{C_{\mathrm{bare}}} \tag{7}$$

Here, $C_{\mathrm{S\text{-}adsorbed},X}$ and C_{bare} are the charge integrations of hydrogen desorption current at the S-adsorbed Pt electrodes after the potential holding/cycling with the certain potential limit, X, and bare Pt electrodes with the corresponding face orientation, respectively.

RF was plotted with respect to the positive potential limit, as shown in Figure 5. Both the potential holding and cycling experiments show that, among the three different face orientations, RF is highest at the Pt(111) electrode throughout the potential range of 0.8−1.0 V, showing that oxidative desorption of sulfur and recovery of ECSA occur at less positive potential than at the Pt(110) and Pt(100) electrodes.

The RFs in Figure 5 show that the recovery from sulfur poisoning is faster at Pt(111) than at Pt(110) and Pt(100) electrodes. To elucidate this difference, theoretical calculations using the DFT were carried out. It is known that the key species for the sulfur oxidation at the Pt surface is SO_2; for example, the DFT study by Yeh and Ho has shown that the activation barriers for S + O → SO and SO + O → SO_2 are 0.44 and 0.41 eV, respectively.[63] These values are much smaller than the desorption energy of SO_2, as will be shown later. In addition, the SO_2 molecule is experimentally observed in our work; thus, it should be considered as the stable species during the sulfur oxidation on Pt surfaces. Considering this, the desorption of SO_2 from Pt surfaces can be assumed to be a thermodynamical bottleneck. Based on the above assumption, the values of adsorption energy (E_{ad}) of SO_2 were calculated with the DFT on Pt(111), Pt(110), and Pt(100); the results are summarized in Table 1. The surface−adsorbate structures are shown in Figure 6. The calculated values of E_{ad} clearly show that the adsorption of SO_2 on Pt(111) is weaker than that at the other two surfaces; the values of E_{ad} are −0.92, −1.41, and −1.35 eV on Pt(111), Pt(110), and Pt(100) (with the optPBE functional), respectively. Although the absolute values of E_{ad} depend on the exchange−correlation functional, the SO_2 adsorption strength is in the order of Pt(110) ≃ Pt(100) ≫ Pt(111) in all the functionals. The weakest SO_2 adsorption on Pt(111) means that the desorption from the surface is favorable on Pt(111), which has been shown by an experimental RF value in Figure 5. Previously, the values of E_{ad} of elemental sulfur on Pt(111), Pt(110), and Pt(100) surfaces were calculated to be −4.63, −4.37, and −5.16 eV, respectively.[64] This order is in contradiction to the experimental observation that the RF value is highest at Pt(111), suggesting that the values of E_{ad} of elemental sulfur are unlikely to be the dominant factor.

Table 1. DFT-Calculated Values of Adsorption Energy (E_{ad}, in eV) of SO_2 on the Pt(111), Pt(110), and Pt(100) Surfaces Estimated by Several Exchange−Correlation Functionals

	E_{ad}/eV				
surface	PBE	PBE + D3	vdw-dft	BEEF	optPBE
(111)	−1.16	−1.81	−0.58	−1.04	−0.92
(110)	−1.64	−2.22	−1.09	−1.57	−1.41
(100)	−1.64	−2.22	−0.87	−1.36	−1.35

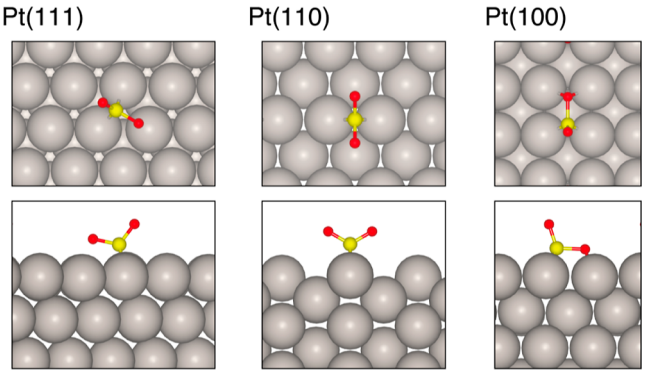

Figure 6. Optimized structures (with the optPBE functional) of SO_2 molecules adsorbed on Pt(111), Pt(110), and Pt(100) (from left to right) surfaces. The top and bottom panels show the top and side views, respectively.

RFs of the Pt(110) and Pt(100) surfaces were almost identical to each other but slightly higher at the Pt(100) surface in the potential holding experiment, while their trend was opposite in the potential cycling experiment. This contradiction should be due to the SO_2 reduction capability of the Pt(100) electrode being higher than those of the Pt(111) and Pt(110) electrodes, as discussed in Figure 3. According to the potential holding experiment (Figure 2), intrinsic sulfur oxidative desorption capabilities were higher at the Pt(111), Pt(100), and Pt(110) electrodes in that order, which is consistent with the adsorption energy of SO_2. In the potential cycling experiment (Figure 4), however, some of the SO_2 oxidatively formed during the positive going scan can be reduced to elemental sulfur (or sulfur interacting with Pt) before further oxidation or diffusion in the bulk solution during the negative going scan. This cycle is more likely to occur at the Pt(100) electrode than at the Pt(111) and Pt(110) electrodes because of its higher SO_2 reduction capability (Figure 3), resulting in the slower recovery of ECSA at the Pt(100) electrode in the potential cycling experiment.

4. CONCLUSIONS

The adsorbed sulfur significantly inhibits the electrochemical responses characteristic to each of the Pt(111), Pt(110), and Pt(100) electrodes, originating from the surface-sensitive processes such as adsorption/desorption of hydrogen and hydroxyl species. The ECSA, which is an important parameter in considering the use of Pt electrodes for fuel cells, gradually recovers by keeping the potential more positive for a longer period because of the oxidative desorption of sulfur species. The adsorbed sulfur is oxidized mainly to SO_2 at 0.7 V vs Ag/AgCl or more positive. Then, some of the SO_2 is further oxidized and/or desorbs from the surface to diffuse into the bulk solution, while the remaining SO_2 can be reverted to the reduced form, i.e., elemental sulfur or sulfur interacting with Pt, at the surface in the negative going scan. Among the elementary steps of the oxidative desorption process of adsorbed sulfur, the desorption

https://doi.org/10.1021/acs.jpcc.4c03227
J. Phys. Chem. C 2024, 128, 16426−16436

of SO_2 from the surface is a very important one that significantly affects the overall rate of the process as well as the oxidation reaction of elemental sulfur and adsorption of oxygen species as an oxygen source. The atomic arrangement of the Pt(111) electrode that has the smallest adsorption energy of SO_2 is the most advantageous for recovery from sulfur poisoning because the desorption of SO_2 formed by the oxidation of elemental sulfur occurs more easily. This makes the recovery of ECSA at a less positive potential as compared to those of Pt(110) and Pt(100) electrodes. Thus, the electrochemical oxidative desorption of sulfur at Pt surfaces was studied using single-crystal electrodes to develop the mitigation materials/techniques against sulfur poisoning, and it was found that (111)-rich and (110)/(100)-poor Pt electrocatalysts can be highly tolerant to sulfur poisoning.

■ ASSOCIATED CONTENT

Supporting Information

The Supporting Information is available free of charge at https://pubs.acs.org/doi/10.1021/acs.jpcc.4c03227.

Quantitative analysis based on XPS shown in Fig. 2D-F a and the theoretical number of atoms and coverage of elemental sulfur at the S-adsorbed Pt(111), Pt(110), and Pt(100) surfaces; SXRD measurements; magnified cyclic voltammograms of Fig. 2 A-C for observing the onset of sulfur oxidation current; and charge integrations of hydrogen desorption current at the S-adsorbed Pt(111), Pt(110), and Pt(100) surfaces after the potential holding/cycling experiment, together with those of bare (PDF)

■ AUTHOR INFORMATION

Corresponding Author

Takuya Masuda − *Research Center for Energy and Environmental Materials (GREEN), National Institute for Materials Science (NIMS), Ibaraki 305-0044, Japan;* orcid.org/0000-0001-7462-2177; Email: MASUDA.Takuya@nims.go.jp

Authors

Tetsuro Morooka − *Research Center for Energy and Environmental Materials (GREEN), National Institute for Materials Science (NIMS), Ibaraki 305-0044, Japan*

Tamao Shishido − *Research Center for Energy and Environmental Materials (GREEN), National Institute for Materials Science (NIMS), Ibaraki 305-0044, Japan*

Ruttala Devivaraprasad − *Research Center for Energy and Environmental Materials (GREEN), National Institute for Materials Science (NIMS), Ibaraki 305-0044, Japan*

Ganesan Elumalai − *Research Center for Energy and Environmental Materials (GREEN), National Institute for Materials Science (NIMS), Ibaraki 305-0044, Japan*

Makoto Aoki − *Research Center for Energy and Environmental Materials (GREEN), National Institute for Materials Science (NIMS), Ibaraki 305-0044, Japan*

Tetsuroh Shirasawa − *Research Institute for Material and Chemical Measurement, National Institute of Advanced Industrial Science and Technology (AIST), Ibaraki 305-8563, Japan;* orcid.org/0000-0001-5519-6977

Takuya Nakanishi − *Research Center for Energy and Environmental Materials (GREEN), National Institute for Materials Science (NIMS), Ibaraki 305-0044, Japan;* orcid.org/0000-0002-1172-718X

Atsushi Ishikawa − *Department of Transdisciplinary Science and Engineering, School of Environment and Society, Tokyo Institute of Technology, Tokyo 152-8552, Japan;* orcid.org/0000-0001-6908-831X

Toshihiro Kondo − *Graduate School of Humanities and Sciences, Ochanomizu University, Tokyo 112-8610, Japan;* orcid.org/0000-0002-5235-7648

Complete contact information is available at: https://pubs.acs.org/10.1021/acs.jpcc.4c03227

Notes

The authors declare no competing financial interest.

■ ACKNOWLEDGMENTS

This paper is based on results obtained from a project, JPNP20003, commissioned by the New Energy and Industrial Technology Development Organization (NEDO). This work was also supported by GteX Program Japan grant number JPMJGX23H0. Synchrotron radiation experiments were performed as projects approved by the High Energy Accelerator Research Organization (KEK) (proposal nos. 2016G588, 2018G620, 2019G668, and 2020G671). We thank Dr. Hironori Nakao for supporting SXRD measurements.

■ REFERENCES

(1) Borup, R.; Meyers, J.; Pivovar, B.; Kim, Y. S.; Mukundan, R.; Garland, N.; Myers, D.; Wilson, M.; Garzon, F.; Wood, D.; et al. Scientific Aspects of Polymer Electrolyte Fuel Cell Durability and Degradation. *Chem. Rev.* **2007**, *107*, 3904−3951.

(2) Debe, M. K. Electrocatalyst approaches and challenges for automotive fuel cells. *Nature* **2012**, *486*, 43−51.

(3) Kodama, K.; Nagai, T.; Kuwaki, A.; Jinnouchi, R.; Morimoto, Y. Challenges in applying highly active Pt-based nanostructured catalysts for oxygen reduction reactions to fuel cell vehicles. *Nat. Nanotechnol.* **2021**, *16*, 140−147.

(4) Garzon, F. H.; Lopes, T.; Rockward, T.; Sansiñena, J. M.; Kienitz, B.; Mukundan, R.; Springer, T. The Impact of Impurities On Long Term PEMFC Performance. *ECS Trans.* **2009**, *25* (1), 1575−1583.

(5) Dong, W.; Xu, C.; Zhao, W.; Xin, M.; Xiang, Y.; Zheng, A.; Dou, M.; Ke, S.; Dong, J.; Qiu, L.; Xu, G. Poisoning Effects of H_2S, CS_2, and COS on Hydrogen Oxidation Reaction over Pt/C Catalysts. *ACS Appl. Energy Mater.* **2022**, *5*, 12640−12650.

(6) Reshetenko, T. V. Impacts of operating conditions on the recovery of proton exchange membrane fuel cells exposed to sulfur dioxide in an air stream. *J. Power Sources* **2023**, *559*, 232676.

(7) Mohtadi, R.; Lee, W.-K.; Cowan, S.; Van Zee, J. W.; Murthy, M. Effects of Hydrogen Sulfide on the Performance of a PEMFC. *Electrochem. Solid-State Lett.* **2003**, *6* (12), A272−A274.

(8) Ke, S.; Qiu, L.; Zhao, W.; Sun, C.; Cui, B.; Xu, G.; Dou, M. Understanding of Correlation between Electronic Properties and Sulfur Tolerance of Pt-Based Catalysts for Hydrogen Oxidation. *ACS Appl. Mater. Interfaces* **2022**, *14*, 7768−7778.

(9) Mohtadi, R.; Lee, W.-K.; Van Zee, J. W. The effect of temperature on the adsorption rate of hydrogen sulfide on Pt anodes in a PEMFC. *Appl. Catal., B* **2005**, *56*, 37−42.

(10) Shi, W.; Yi, B.; Hou, M.; Jing, F.; Ming, P. Hydrogen sulfide poisoning and recovery of PEMFC Pt-anodes. *J. Power Sources* **2007**, *165*, 814−818.

(11) Jerkiewicz, G.; Borodzinski, J. J.; Chrzanowskia, W.; Conway, B. E. Examination of factors influencing promotion of H absorption into metals by site-blocking elements. *J. Electrochem. Soc.* **1995**, *142*, 3755−3763.

(12) Zolfaghari, A.; Jerkiewicz, G.; Chrzanowski, W.; Wieckowski, A. Energetics of the underpotential deposition of hydrogen on platinum electrodes II. Presence of coadsorbed sulfur. *J. Electrochem. Soc.* **1999**, *146*, 4158−4165.

(13) Batina, N.; McCargar, J. W.; Salaita, G. N.; Lu, F.; Laguren-Davidson, L.; Lin, C.-H.; Hubbard, A. T. Structure and composition of platinum(111) and platinum(100) surfaces as a function of electrode potential in aqueous sulfide solutions. *Langmuir* **1989**, *5*, 123−128.
(14) Marcus, P.; Protopopoff, E. Coadsorption of sulphur and hydrogen on platinum (110) studied by radiotracer and electrochemical techniques. *Surf. Sci.* **1985**, *161*, 533−552.
(15) Maurice, V.; Marcus, P. STM imaging in air with atomic resolution of adsorbates on metal surfaces: Pt(100)-c(2 × 2)s. *Surf. Sci. Lett.* **1992**, *262*, L59−L64.
(16) McIntyre, B. J.; Sautet, P.; Dunphy, J. C.; Salmeron, M.; Somorjai, G. A. Scanning tunneling microscopy tip-dependent image contrast of S/Pt(111) by controlled atom transfer. *J. Vac. Sci. Technol. B* **1994**, *12*, 1751−1753.
(17) Yoon, H. A.; Materer, N.; Salmeron, M.; Van Hove, M. A.; Somorjai, G. A. Coverage-dependent structures of sulfur on Pt(111) studied by low-energy electron diffraction (LEED) and scanning tunneling microscopy (STM). *Surf. Sci.* **1997**, *376*, 254−266.
(18) Gould, B. D.; Baturina, O. A.; Swider-Lyons, K. E. Deactivation of Pt/VC proton exchange membrane fuel cell cathodes by SO_2, H_2S and COS. *J. Power Sources* **2009**, *188*, 89−95.
(19) Fu, J.; Hou, M.; Du, C.; Shao, Z.; Yi, B. Potential dependence of sulfur dioxide poisoning and oxidation at the cathode of proton exchange membrane fuel cells. *J. Power Sources* **2009**, *187*, 32−38.
(20) Ramaker, D. E.; Gatewood, D.; Korovina, A.; Garsany, Y.; Swider-Lyons, K. E. Resolving Sulfur Oxidation and Removal from Pt and Pt_3Co Electrocatalysts Using in Situ X-ray Absorption Spectroscopy. *J. Phys. Chem. C* **2010**, *114*, 11886−11897.
(21) Park, I.-S.; Xu, B.; Atienza, D. O.; Hofstead-Duffy, A. M.; Allison, T. C.; Tong, Y. J. Chemical State of Adsorbed Sulfur on Pt Nanoparticles. *ChemPhysChem* **2011**, *12*, 747−752.
(22) Awad, M. I.; Saleh, M. M.; Ohsaka, T. Electroactivity regeneration of sulfur-poisoned platinum nanoparticle-modified glassy carbon electrode at low anodic potentials. *J. Solid State Electrochem.* **2015**, *19*, 1331−1340.
(23) Potgieter, M.; Parrondo, J.; Ramani, V. K.; Kriek, R. J. Evaluation of Polycrystalline Platinum and Rhodium Surfaces for the Electro-Oxidation of Aqueous Sulfur Dioxide. *Electrocatalysis* **2016**, *7*, 50−59.
(24) Sung, Y.-E.; Chrzanowski, W.; Zolfaghari, A.; Jerkiewicz, G.; Wieckowski, A. Structure of Chemisorbed Sulfur on a Pt(111) Electrode. *J. Am. Chem. Soc.* **1997**, *119*, 194−200.
(25) Sung, Y.-E.; Chrzanowski, W.; Wieckowski, A.; Zolfaghari, A.; Blais, S.; Jerkiewicz, G. Coverage evolution of sulfur on Pt(111) electrodes: From compressed overlayers to well-defined islands. *Electrochim. Acta* **1998**, *44*, 1019−1030.
(26) Chen, C.-H.; Halford, A.; Walker, M.; Brennan, C.; Lai, S. C. S.; Fermin, D. J.; Unwin, P. R.; Rodriguez, P. Electrochemical characterization and regeneration of sulfur poisoned Pt catalysts in aqueous media. *J. Electroanal. Chem.* **2018**, *816*, 138−148.
(27) Kattwinkel, L.; Magnussen, O. M. Optical reflectance studies on the oxidation of chemisorbed sulfur at the Pt(111) electrode. *Electrochim. Acta* **2022**, *434*, 141297.
(28) Masuda, T.; Fukumitsu, H.; Kondo, T.; Naohara, H.; Tamura, K.; Sakata, O.; Uosaki, K. Structure of Pt(111)/Ionomer Membrane Interface and Its Bias-Induced Change in Membrane Electrode Assembly. *J. Phys. Chem. C* **2013**, *117*, 12168−12171.
(29) Masuda, T.; Sonsudin, F.; Singh, P. R.; Naohara, H.; Uosaki, K. Potential-Dependent Adsorption and Desorption ofPerfluorosulfonated Ionomer on a Platinum Electrode SurfaceProbed by Electrochemical Quartz Crystal Microbalance and AtomicForce Microscopy. *J. Phys. Chem. C* **2013**, *117*, 15704−15709.
(30) Clavilier, J. Flame-annealing and cleaning technique. *Interfacial electrochemistry: theory, experiment, and applications*; Wieckowski, A., Ed.; Marcel Dekker: New York, 1999; pp 231−248.
(31) Kondo, T.; Tamura, K.; Takahashi, M.; Mizuki, J.; Uosaki, K. A novel spectroelectrochemical cell for in situ surface X-ray scattering measurements of single crystal disk electrodes. *Electrochim. Acta* **2002**, *47*, 3075−3080.
(32) Shatkay, A.; Lerman, A. Individual activities of sodium and chloride ions in aqueous solutions of sodium chloride. *Anal. Chem.* **1969**, *41*, 514−517.
(33) Rabie, H. R.; Wilczek-Vera, G.; Vera, J. H. Activities of individual ions from infinite dilution to saturated solutions. *J. Solution Chem.* **1999**, *28*, 885−913.
(34) Masuda, T.; Uosaki, K. In situ determination of electronic structure at solid/liquid interfaces. *J. Electron Spectrosc. Relat. Phenom.* **2017**, *221*, 88−98.
(35) Collard, S. M.; McLellan, R. B. High-temperature elastic constants of platinum single crystals. *Acta Metall. Mater.* **1992**, *40*, 699−702.
(36) Ungerer, M. J.; Santos-Carballal, D.; Cadi-Essadek, A.; van Sittert, C. G. C. E.; de Leeuw, N. H. Interaction of SO2 with the Platinum (001), (011), and (111) Surfaces: A DFT Study. *Catalysts* **2020**, *10*, 558.
(37) Blöchl, P. E. Projector augmented-wave method. *Phys. Rev. B* **1994**, *50*, 17953−17979.
(38) Perdew, J. P.; Burke, K.; Ernzerhof, M. Generalized Gradient Approximation Made Simple. *Phys. Rev. Lett.* **1996**, *77*, 3865−3868.
(39) Grimme, S.; Ehrlich, S.; Goerigk, L. Effect of the damping function in dispersion corrected density functional theory. *J. Comput. Chem.* **2011**, *32*, 1456−1465.
(40) Dion, M.; Rydberg, H.; Schröder, E.; Langreth, D. C.; Lundqvist, B. I. *Phys. Rev. Lett.* **2004**, *92*, 246401.
(41) Wellendorff, J.; Lundgaard, K. T.; Møgelhøj, A.; Petzold, V.; Landis, D. D.; Nørskov, J. K.; Bligaard, T.; Jacobsen, K. W. Density functionals for surface science: Exchange-correlation model development with Bayesian error estimation. *Phys. Rev. B* **2012**, *85*, 235149.
(42) Klimeš, J.; Bowler, D. R.; Michaelides, A. Chemical accuracy for the van der Waals density functional. *J. Phys.: Condens. Matter* **2010**, *22*, 022201.
(43) Perdew, J. P.; Ruzsinszky, A.; Csonka, G. I.; Vydrov, O. A.; Scuseria, G. E.; Constantin, L. A.; Zhou, X.; Burke, K. Restoring the Density-Gradient Expansion for Exchange in Solids and Surfaces. *Phys. Rev. Lett.* **2008**, *100*, 136406.
(44) Kresse, G.; Furthmüller, J. Efficient iterative schemes for ab initio total-energy calculations using a plane-wave basis set. *Phys. Rev. B* **1996**, *54*, 11169−11186.
(45) Kresse, G.; Furthmüller, J. Efficiency of ab-initio total energy calculations for metals and semiconductors using a plane-wave basis set. *Comput. Mater. Sci.* **1996**, *6*, 15−50.
(46) Momma, K.; Izumi, F. VESTA: a three-dimensional visualization system for electronic and structural analysis. *J. Appl. Crystallogr.* **2008**, *41*, 653−658.
(47) Boronat-González, A.; Herrero, E.; Feliu, J. M. Determination of the potential of zero charge of Pt/CO electrodes using an impinging jet system. *J. Solid State Electrochem.* **2020**, *24*, 2871−2881.
(48) Rodriguez, J. A.; Kuhn, M.; Hrbek, J. The bonding of sulfur to a Pt(111) surface: photoemission and molecular orbital studies. *Chem. Phys. Lett.* **1996**, *251*, 13−19.
(49) Yang, Z.; Wu, R.; Rodriguez, J. A. First-principles study of the adsorption of sulfur on Pt(111): S core-level shifts and the nature of the Pt-S bond. *Phys. Rev. B* **2002**, *65*, 155409.
(50) Rodriguez, J. A.; Dvorak, J.; Jirsak, T.; Liu, G.; Hrbek, J.; Aray, Y.; González, C. Coverage Effects and the Nature of the Metal-Sulfur Bond in S/Au(111): High-Resolution Photoemission and Density-Functional Studies. *J. Am. Chem. Soc.* **2003**, *125*, 276−285.
(51) Wakisaka, M.; Udagawa, Y.; Suzuki, H.; Uchida, H.; Watanabe, M. Structural effects on the surface oxidation processes at Pt single-crystal electrodes studied by X-ray photoelectron spectroscopy. *Energy Environ. Sci.* **2011**, *4*, 1662−1666.
(52) Quijada, C.; Vázquez, J. L.; Pérez, J. M.; Aldaz, A. Voltammetric behaviour of irreversibly adsorbed SO_2 on a Pt(111) electrode in sulphuric acid medium. *J. Electroanal. Chem.* **1994**, *372*, 243−250.
(53) Wakisaka, M.; Asizawa, S.; Uchida, H.; Watanabe, M. In situ STM observation of morphological changes of the Pt(111) electrode surface during potential cycling in 10 mM HF solution. *Phys. Chem. Chem. Phys.* **2010**, *12*, 4184−4190.

https://doi.org/10.1021/acs.jpcc.4c03227
J. Phys. Chem. C 2024, 128, 16426−16436

(54) Matsumoto, M.; Miyazaki, T.; Imai, H. Oxygen-Enhanced Dissolution of Platinum in Acidic Electrochemical Environments. *J. Phys. Chem. C* **2011**, *115*, 11163−11169.
(55) Conway, B. E.; Barnett, B.; Angerstein-Kozlowska, H.; Tilak, B. V. A surface-electrochemical basis for the direct logarithmic growth law for initial stages of extension of anodic oxide films formed at noble metals. *J. Chem. Phys.* **1990**, *93*, 8361−8373.
(56) Komanicky, V.; Chang, K. C.; Menzel, A.; Markovic, N. M.; You, H.; Wang, X.; Myers, D. Stability and Dissolution of Platinum Surfaces in Perchloric Acid. *J. Electrochem. Soc.* **2006**, *153*, B446−B451.
(57) Streber, R.; Papp, C.; Lorenz, M. P. A.; Hofert, O.; Zhao, W.; Wickert, S.; Darlatt, E.; Bayer, A.; Denecke, R.; Steinrück, H. P. Influence of Steps on the Adsorption and Thermal Evolution of SO2 on Clean and Oxygen Precovered Pt Surfaces. *J. Phys. Chem. C* **2010**, *114*, 19734−19743.
(58) Sonsudin, F.; Masuda, T.; Ikeda, K.; Naohara, H.; Uosaki, K. Effect of Coating by Perfluorosulfonated Ionomer Film on Electrochemical Behaviors of Pt(111) Electrode in Acidic Solutions. *Chem. Lett.* **2010**, *39*, 286−287.
(59) Itaya, K.; Sugawara, S.; Sashikata, K.; Furuya, N. In situ scanning tunneling microscopy of platinum (111) surface with the observation of monatomic steps. *J. Vac. Sci. Technol., A* **1990**, *8*, 515−519.
(60) Sashikata, K.; Furuya, N.; Itaya, K. In situ electrochemical scanning tunneling microscopy of single-crystal surfaces of Pt(111), Rh(111), and Pd(111) in aqueous sulfuric acid solution. *J. Vac. Sci. Technol. B* **1991**, *9*, 457−464.
(61) Nagy, Z.; You, H. Applications of surface X-ray scattering to electrochemistry problems. *Electrochim. Acta* **2002**, *47*, 3037−3055.
(62) Herrero, E.; Climent, V.; Feliu, J. M. On the different adsorption behavior of bismuth, sulfur, selenium and tellurium on a Pt(775) stepped surface. *Electrochem. Commun.* **2000**, *2*, 636−640.
(63) Yeh, C.-H.; Ho, J.-J. A First-Principle Calculation of Sulfur Oxidation on Metallic Ni(111) and Pt(111), and Bimetallic Ni@Pt(111) and Pt@Ni(111) Surfaces. *ChemPhysChem* **2012**, *13*, 3194−3203.
(64) Bernard Rodriguez, C. R.; Santana, J. A. Adsorption and diffusion of sulfur on the (111), (100), (110), and (211) surfaces of FCC metals: Density functional theory calculations. *J. Chem. Phys.* **2018**, *149*, 204701.

https://doi.org/10.1021/acs.jpcc.4c03227
J. Phys. Chem. C 2024, 128, 16426−16436